Since January 2020 Elsevier has created a COVID-19 resource centre with free information in English and Mandarin on the novel coronavirus COVID-19. The COVID-19 resource centre is hosted on Elsevier Connect, the company's public news and information website.

Science of the Total Environment 757 (2021) 143823

Contents lists available at ScienceDirect

Science of the Total Environment

journal homepage: www.elsevier.com/locate/scitotenv

Impact of COVID-19 lockdown on ambient levels and sources of volatile organic compounds (VOCs) in Nanjing, China

Ming Wang [a], Sihua Lu [b], Min Shao [c,*], Limin Zeng [b], Jun Zheng [a], Fangjian Xie [d], Haotian Lin [a], Kun Hu [a], Xingdong Lu [a]

[a] Collaborative Innovation Center of Atmospheric Environment and Equipment Technology, Jiangsu Key Laboratory of Atmospheric Environment Monitoring and Pollution Control, School of Environmental Science and Engineering, Nanjing University of Information Science & Technology, Nanjing 210044, China
[b] College of Environmental Sciences and Engineering, Peking University, Beijing 100871, China
[c] Institute for Environmental and Climate Research, Jinan University, Guangzhou 511443, China
[d] Nanjing Municipal Academy of Ecological and Environment Protection Science, Nanjing 210093, China

HIGHLIGHTS

- NMHCs level and reactivity decreased by 46% and 61% during COVID-19 lockdown.
- NMHCs levels from petrochemical industry and traffic decreased by 80% and 67%.
- NMHCs and NO_2 dropped during lockdown, but O_3 formation rate did not decrease.

GRAPHICAL ABSTRACT

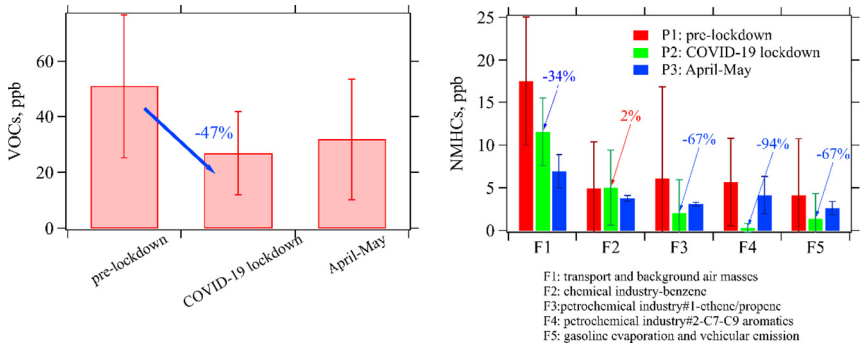

ARTICLE INFO

Article history:
Received 3 September 2020
Received in revised form 16 October 2020
Accepted 1 November 2020
Available online 20 November 2020

Editor: Jianmin Chen

Keywords:
COVID-19
VOCs
Source apportionment
Industrial emission
Ozone
Nanjing

ABSTRACT

A lot of restrictive measures were implemented in China during January–February 2020 to control rapid spread of COVID-19. Many studies reported impact of COVID-19 lockdown on air quality, but little research focused on ambient volatile organic compounds (VOCs) till now, which play important roles in production of ozone and secondary organic aerosol. In this study, impact of COVID-19 lockdown on VOCs mixing ratios and sources were assessed based on online measurements of VOCs in Nanjing during December 20, 2019-Feburary 15, 2020 (P1-P2) and April 15–May 13, 2020 (P3). Average VOCs levels during COVID-19 lockdown period (P2) was 26.9 ppb, about half of value for pre-lockdown period (P1). Chemical composition of VOCs also showed significant changes. Aromatics contribution during decreased from 13% during P1 to 9% during P2, whereas alkanes contribution increased from 64% to 68%. Positive matrix factorization (PMF) was then applied for non-methane hydrocarbons (NMHCs) sources apportionment. Five sources were identified, including a source related to transport and background air masses, three sources related to petrochemical industry or chemical industry (*petrochemical industry#1-propene/ethene*, *petrochemical industry#2-C7-C9 aromatics*, and *chemical industry-benzene*), and a source attributed to gasoline evaporation and vehicular emission. During P2, NMHCs levels from *petrochemical industry#2-C7-C9 aromatics* showed the largest relative decline of 94%, followed by *petrochemical industry#1-propene/ethene* (67%), and *gasoline evaporation and vehicular emission* (67%). Furthermore, ratios of OH reactivity of NMHCs *versus* NO_2 level ($R_{OH,NMHCs}/NO_2$) and total oxidant production rate ($P(O_X)$) were calculated to assess potential influences of COVID-19 lockdown on O_3 formation.

* Corresponding author.
E-mail address: mshao@pku.edu.cn (M. Shao).

https://doi.org/10.1016/j.scitotenv.2020.143823
0048-9697/

1. Introduction

From December 2019, the coronavirus disease (COVID-19) spread worldwide and caused enormous influences on international economy, industrial production, and social life. To prevent COVID-19 pandemic and protect human health, 30 provinces of China started the Level I (particularly serious) response to public health emergencies from 23rd to 25th January 2020. A lot of restrictive measures were implemented to reduce people's social contacts, such as shutting down theatres, restaurants, malls, schools, and non-essential businesses, restricting public transportation (*e.g.* airplane, train, and bus) and even private cars, *etc.* More detailed descriptions on National Emergency Response Plan for Public Emergencies can be found in the paper by Li et al. (2020). Anthropogenic sources related to human activities (*e.g.* traffic-related emissions, industrial emissions) were considered as the largest contributor to air pollutants in urban areas (Lelieveld et al., 2015), and therefore COVID-19 lockdown will result in reduction of anthropogenic air pollutants emissions (Huang et al., 2020; Li et al., 2020).

The latest research publications have reported the significant impact of COVID-19 lockdown on air qualities in China (Chen et al., 2020; Li et al., 2020), United States (Zangari et al., 2020), Europe (Menut et al., 2020), India (Kumari and Toshniwal, 2020), and other regions (Kondo Nakada and Urban, 2020). Based on ground and satellite measurement results, concentrations of fine particle ($PM_{2.5}$), sulfur dioxide (SO_2), and nitrogen dioxide (NO_2) exhibited significant declines in many cities (Bauwens et al., 2020; Chauhan and Singh, 2020; Rodriguez-Urrego and Rodriguez-Urrego, 2020; Zangari et al., 2020), whereas surface ozone (O_3) pollution was amplified (Sicard et al., 2020; Zhao et al., 2020) during COVID-19 lockdown period. Volatile organic compounds (VOCs) are important precursors of O_3 and $PM_{2.5}$ (Atkinson et al., 2006), but variations of ambient VOCs levels caused by COVID-19 lockdown are still unclear until now.

Compared with inorganic air pollutants, *e.g.* NO_X and SO_2, ambient VOCs have various chemical composition and wide sources (Li et al., 2019). It is essential to obtain accurate knowledge of VOCs sources in order to reduce their emissions and improve air quality. A few studies based on emission inventory and receptor models have been conducted to determine ambient VOCs sources in Nanjing, China (An et al., 2017; Zhao et al., 2017; Wang et al., 2020a). Transportation and industry were considered as the two largest contributors to ambient VOCs, whereas relative contributions of individual sources to VOCs showed some discrepancies among different studies. In the emission inventory built by Zhao et al. (2017), industrial processing and solvent use were considered as the most important VOCs sources, with relative contributions of 50% and 31%, respectively. However, two receptor model studies based on ambient measurements suggested that transportation and fuels combustion were also important sources of VOCs, with relative contributions of 39%–51% (An et al., 2017; Wang et al., 2020a). During COVID-19 lockdown period, traffic flow decreased and most industrial production processes stagnated, and thus VOCs emissions from transportation and industry reduced significantly (Huang et al., 2020; Li et al., 2020). This provides an opportunity for us to further understand and evaluate VOCs sources in Nanjing.

The Yangtze River Delta (YRD) region started the Level I response to public health emergencies on 00:00 of 25th January 2020 and then adjusted to Level II (serious) response in 25th February 2020. In this study, online measurements of ambient VOCs were conducted during about 3 months to evaluate impact of COVID-19 lockdown on VOCs mixing ratios and sources in Nanjing. Temporal variations of VOCs levels were analyzed, and then ratio analysis and positive matrix factorization (PMF) model were applied for VOCs source apportionment. Changes of VOCs levels from individual sources were then investigated to evaluate impact of COVID-19 lockdown on industrial and traffic-related VOCs emissions. Furthermore, ratios for VOCs reactivity *versus* NO_2 levels were calculated and their implications on O_3 formation mechanism were discussed.

2. Methodology

2.1. Observation site and period

Online VOCs measurements were conducted in the campus of Nanjing University of Information & Science Technology (NUIST, 118.7°E, 32.2°N, Fig. 1) during December 20th, 2019-Feburary 15th, 2020 and April 15th-May 13rd, 2020. The entire observation period was divided into three stages, including December 20th, 2019-January 24th, 2020 (P1, pre-lockdown), January 25th-Feburary 15th, 2020 (P2, Level I respond period, *i.e.* COVID-19 lockdown), and April 15th-May 13rd, 2020 (Level III response period, P3).

The NUIST site is located in the west of YRD region, about 18 km north from an urban site (JEMC) in downtown area of Nanjing (Fig. 1). There are two expressways close to the NUIST site, especially the expressway in east with about 1 km distance which has large traffic flow every day. Additionally, it should be noted that there are three large petrochemical and chemical industrial areas in east (B), northeast (A), and southeast (C) of this site, with distances of about 5 km, 10 km, and 20 km, respectively. Therefore, this site was considered to be representative of an atmospheric environment influenced by both transportation and petrochemical/chemical industry.

2.2. VOCs measurements

In this study, ambient mixing ratios of 102 VOC species were online measured by a cryogen-free gas chromatography system (GC) equipped with a mass spectrometer detector (MSD) and a flame ionization detector (FID) developed by Peking University. Briefly, target compounds were enriched at a ultra-low temperature of −160 °C, and then they were vapored and injected into GC system for separation and detection. Two parallel channels were designed in the GC–MSD/FID system. In one channel, C2-C5 non-methane hydrocarbons (NMHCs) were trapped using a PLOT (Al_2O_3/KCl) column (25 cm, 0.53 mm ID). After sampling, the enrichment trap was heated to 110 °C and then vaporized compounds were separated by a PLOT (Al_2O_3/KCl) column (15 m, 0.32 mm ID) and detected by an FID. In the other channel, a deactivated quartz capillary (25 cm, 0.53 mm ID) was applied for trapping C5-C12 NMHCs, halocarbons, and oxygenated VOCs (OVOCs). A DB-624 column (30 m, 0.25 mm ID) connected with MSD was employed to separate and detect these compounds. Two commercial mixture standards with 56 C2-C12 NMHCs and 63 chemicals (Spectra Gases, U.S.) were used for calibration. To correct the drift of MSD responses, internal standards were also employed to calculate ambient mixing ratios of VOCs. More detailed introductions on this GC–MSD/FID system and quality assurance and quality control (QA/QC) procedures of VOCs measurements can be found in the paper by Wang et al. (2014).

2.3. Air quality and meteorological conditions

The hourly-averaged concentrations of $PM_{2.5}$, O_3, NO_2, CO, and SO_2 were obtained from the real-time release platform of national urban air quality (http://106.37.208.233:20035/) belonging to the China National Environmental Monitoring Centre (CNEMC). Ambient temperature (T), wind direction and speed (WD and WS), relative humidity (RH), atmospheric pressure (P), and visibility were measured by an automatic weather station in the meteorological observation base of NUIST.

Figs. S1 and S2 show time series of NO_2, O_3, SO_2, CO concentrations and wind vector, temperature, pressure, RH, and visibility. Their comparisons among P1, P2, and P3 were summarized in Table 1. It can be found that temperature, WS, and visibility increased from P1 to P3, whereas RH showed a decline trend. Average concentrations for $PM_{2.5}$, CO, SO_2, and NO_2 during P2 decreased by 12%–48% compared with respective values for P1. However, average concentration of O_3 and total oxidants ($O_X = O_3 + NO_2$) during P2 increased by 92% and 7% *versus*

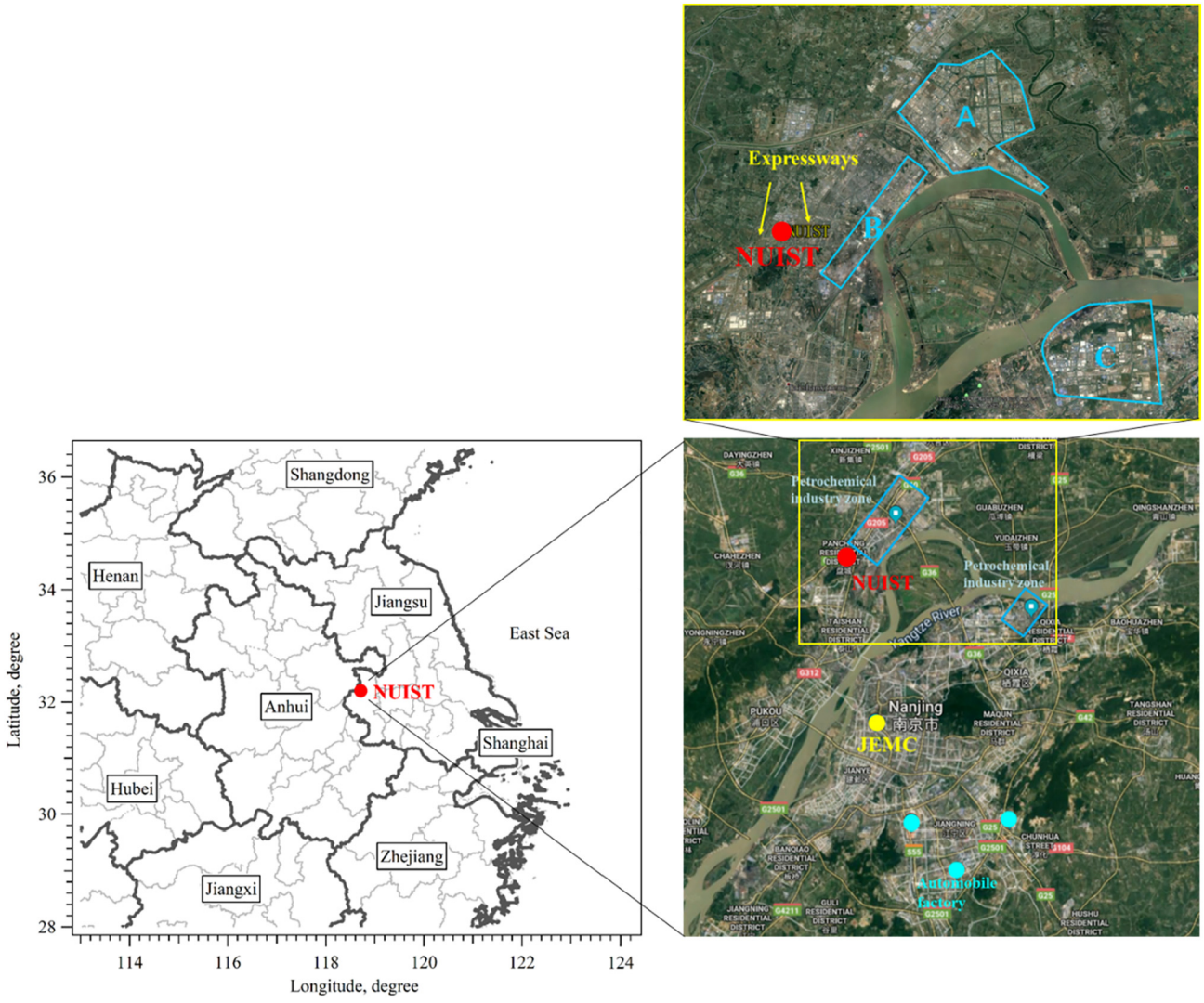

Fig. 1. Location of ambient VOCs measurement site (NUIST) in this study.

P1, respectively. Wind rose plots in Fig. S4 suggest that east was the prevailing wind direction during P1 and P2, while wind was mainly from east and southeast during P3. Back trajectory analysis of air masses indicates that east and north were the dominant directions during P1 and P2, whereas south and southwest were also important air mass trajectories during P3 (Fig. S5). Overall, meteorological conditions during P1 and P2 were similar, but showed a significant discrepancy with those for P3.

Table 1
Comparisons of meteorological parameters and concentrations of trace gases and $PM_{2.5}$ and mixing ratios of VOCs during P1, P2, and P3.

Variables		P1	P2	P3	(P2-P1)/P1 × 100%	*t*-Test (*p*)
Meteorological parameters	WS, m/s	1.62	1.75	3.02	8%	0.031
	Temperature, °C	5.57	6.98	19.5	25%	<0.001
	RH, %	81.8	75	68.8	−8%	<0.001
	Pressure, hPa	102.4	102.2	101.1	0%	<0.001
	Visibility, km	6.23	9.89	14.8	59%	<0.001
Trace gases and $PM_{2.5}$, μg/m^3	$PM_{2.5}$	65.0	42.28	35.9	−35%	<0.001
	CO	0.868	0.764	0.866	−12%	<0.001
	SO_2	8.80	6.3	9.72	−28%	<0.001
	NO_2	49.0	25.7	45.1	−48%	<0.001
	O_3	30.7	59.2	84.9	92%	<0.001
	Ox	79.6	84.8	127	7%	<0.001
VOCs, ppb	VOCs	50.9	26.9	31.9	−47%	<0.001
	NMHCs	38.7	20.9	22.3	−46%	<0.001
	Alkanes	24.6	14.2	13.6	−42%	<0.001
	Alkenes	9.09	4.76	5.11	−48%	<0.001
	Aromatics	5.02	1.90	3.56	−62%	<0.001

3. Results and discussion

3.1. Decrease of VOCs levels during COVID-19 lockdown period

Average concentration of total measured VOC species (VOCs) during P2 was 26.9 ± 14.9 ppb, significantly lower than values for P1 (50.9 ± 25.7 ppb) and P3 (31.9 ± 21.7 ppb). Considering that meteorological parameters during April–May (P3) were different with December–February (P1 and P2), further discussions about impact of COVID-19 lockdown on VOCs levels mainly focused on comparisons between P1 and P2. Relative declines of average alkanes, alkenes, and aromatics levels during P2 *versus* P1 were 42%, 48%, and 62%, respectively (Table 1). *m,p*-Xylene and propene were chosen as representative species because they have been found to be key species in O_3 formation of Nanjing and were influenced significantly by industrial emission (Wang et al., 2020b). Fig. 2 compares temporal variations and frequency histograms of mixing ratios for *m,p*-xylene and propene between P1 and P2. It can be found that levels of *m,p*-xylene and propene both showed large fluctuations. For example, mixing ratio of *m,p*-xylene at 00:00 of January 5th reached 4.47 ppb, and then decreased rapidly to 1.19 ppb at 06:00 of January 5th. For propene, its level at 05:00 of January 2nd reached 22.02 ppb, and then decreased to 0.31 ppb at 13:00 of January 2nd. Such sharp fluctuations cannot be explained by meteorological conditions. Frequency histograms of mixing ratios for *m,p*-xylene and propene were both lognormal distributions. Compared with acetylene which was considered mainly from incomplete combustion sources (Baker et al., 2008), histograms for *m,p*-xylene and propene showed larger tails that extended toward higher values (Fig. S3 of Supplement). Considering the NUIST site is close to the largest petrochemical/chemical industrial zone (A in Fig. 1) in Nanjing, it was considered that ambient *m,p*-xylene and propene were possibly influenced by nearby industrial emissions. The lognormal fitting center (x_0) of *m,p*-xylene mixing ratios during P2 was 0.073 ppb, about one quarter of value for P1. The x_0 for propene mixing ratios was 0.081 ppb during P2, lower than that for P1 by 46%.

Fig. 3 shows average mixing ratios for individual VOC species during P1 and P2, and their relative differences (RD) between these two periods ((P1-P2)/P1). Mixing ratios of long-lived halocarbons, *e.g.* Freon 114 (F114), Freon 113 (F113), and carbon tetrachloride (CCl_4), showed the lowest RD values (<0.1). This is because industrial production and use of these chlorofluorocarbons (CFCs) have been forbidden in China, and therefore their ambient levels kept relatively stable during the entire measurement period. In addition, ethane, benzene, and acetylene mixing ratios also showed relatively low RD values of 0.23–0.32. The possible explanation for this phenomenon is that these species also have long atmospheric lifetimes and thus they would be influenced by transport and background air masses. Except for these species, mixing ratios for other VOCs all showed significant decreases during P2, with RD values of 0.4–0.92, suggesting the possible impact of COVID-19 lockdown on VOCs.

To illustrate the decline of VOCs levels during P2 *versus* P1 was not an accidental event, wintertime VOCs measurement results in Nanjing reported from previous studies (An et al., 2017; Wang et al., 2020a) were also compared with average NMHCs mixing ratios during P2. In the study by An et al. (2017), VOCs were measured in January–February 2014 at the NUIST site (NUIST-2014). Another study by Wang et al. (2020a), VOCs were observed during January–February 2016 at the JEMC site (JEMC-2016). As shown in Table S1 and Fig. S6 of Supplement, average levels for total measured NMHCs and individual species except for ethane and benzene during P2 were all significantly lower than results from NUIST-2014 and JEMC-2016 ($p < 0.01$), with relative decreases of 25%–97%. This finding demonstrates that COVID-19 lockdown is a main cause of the significant declines of VOCs levels during P2.

3.2. Changes of NMHCs chemical compositions and sources

3.2.1. Chemical compositions and ratios of ambient NMHCs

Chemical compositions of NMHCs during P1, P2, and P3 were compared in Fig. S7 of Supplement. Alkanes was the dominant contributor to ambient NMHCs levels during three periods, with relative contributions of 61%–68%. Relative contribution of aromatics decreased from 13% during P1 to 9% during P2, while relative contribution of alkanes increased from 64% to 68%. During P3, fraction of alkanes decreased to

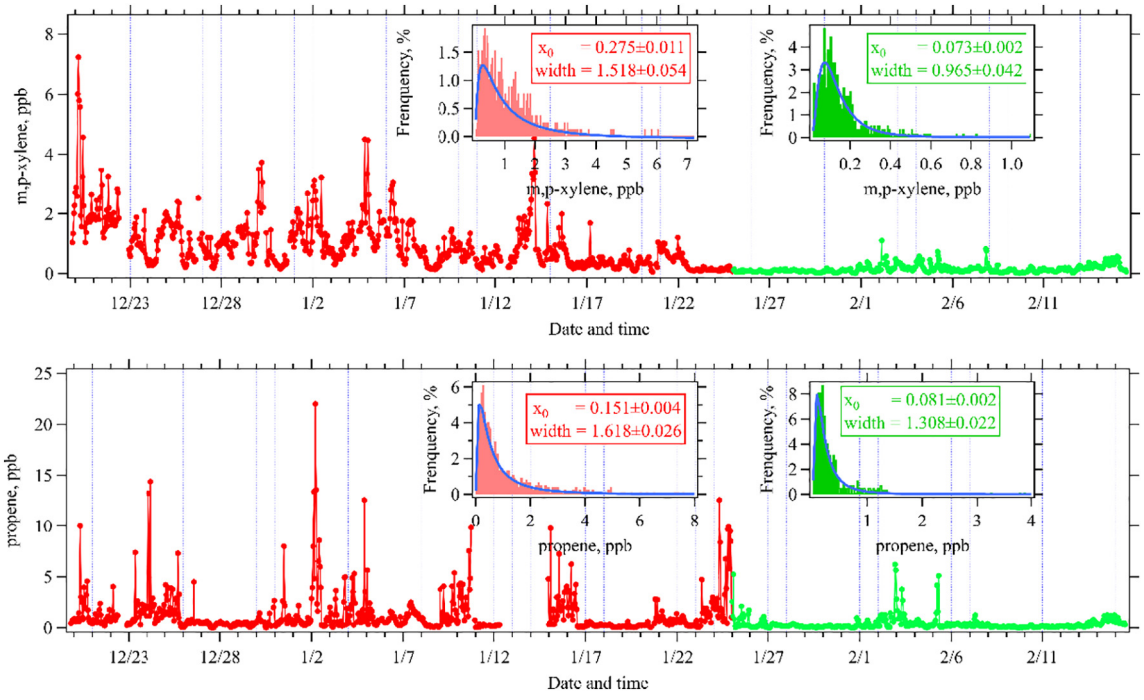

Fig. 2. Time series and frequency histograms of ambient mixing ratios of *m,p*-xylene and propene during P1 and P2.

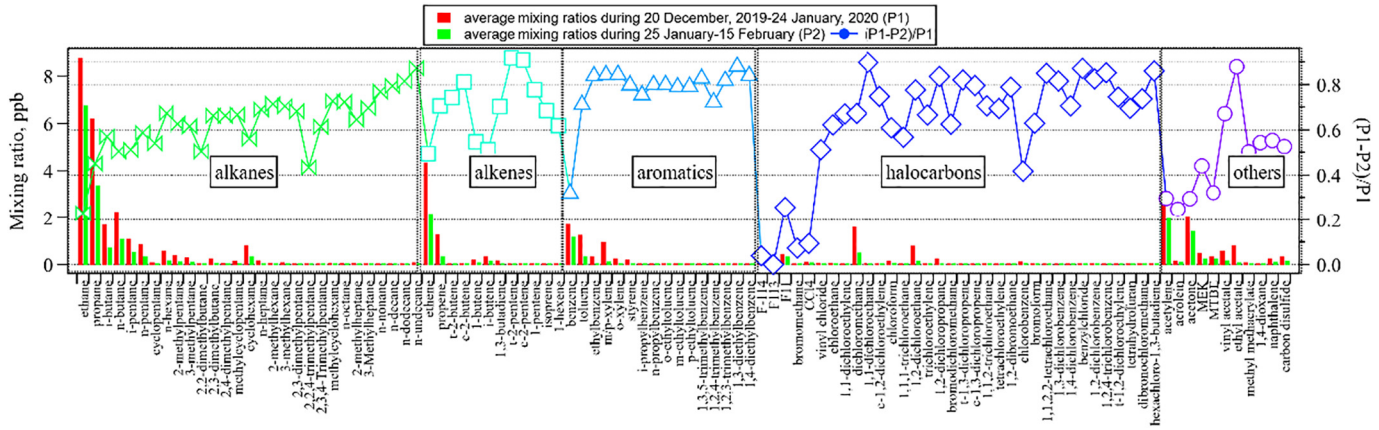

Fig. 3. Average mixing ratios for individual VOC species during P1 and P2 and their relative decreases during P2 *versus* P1 ((P1-P1)/P2).

61%, whereas fraction of aromatics increased to 16%. The difference of NMHCs chemical composition between P1 and P2 indicates possible changes of NMHCs sources resulted from COVID-19 lockdown.

Fig. 4 shows ternary plots for mixing ratios of C2-C4 alkanes, C3-C5 alkanes, C2-C3 alkenes/alkynes, and C6-C8 aromatics. As shown in Fig. 4a, average fraction of ethane in the sum of ethane, propane, and *n*-butane levels increased from 51% during P1 to 60% during P2, whereas fractions of propane and *n*-butane decreased to 30% and 10% during P2, respectively. Ambient propane can be influenced by industrial use of liquefied petroleum gas (LPG) in Nanjing (Wang et al., 2020a). C4-C5 alkanes are important constitutes of VOCs from vehicular exhaust and gasoline evaporation (Gentner et al., 2013; Song et al., 2020). The decline of propane and *n*-butane fractions suggests that contributions of industrial LPG use and traffic-related sources might reduce due to COVID-19 lockdown. For C3-C5 alkanes, average fraction of pentanes (*i.e.* the sum of *n*-pentane and *i*-pentane) increased from 15%–16% for

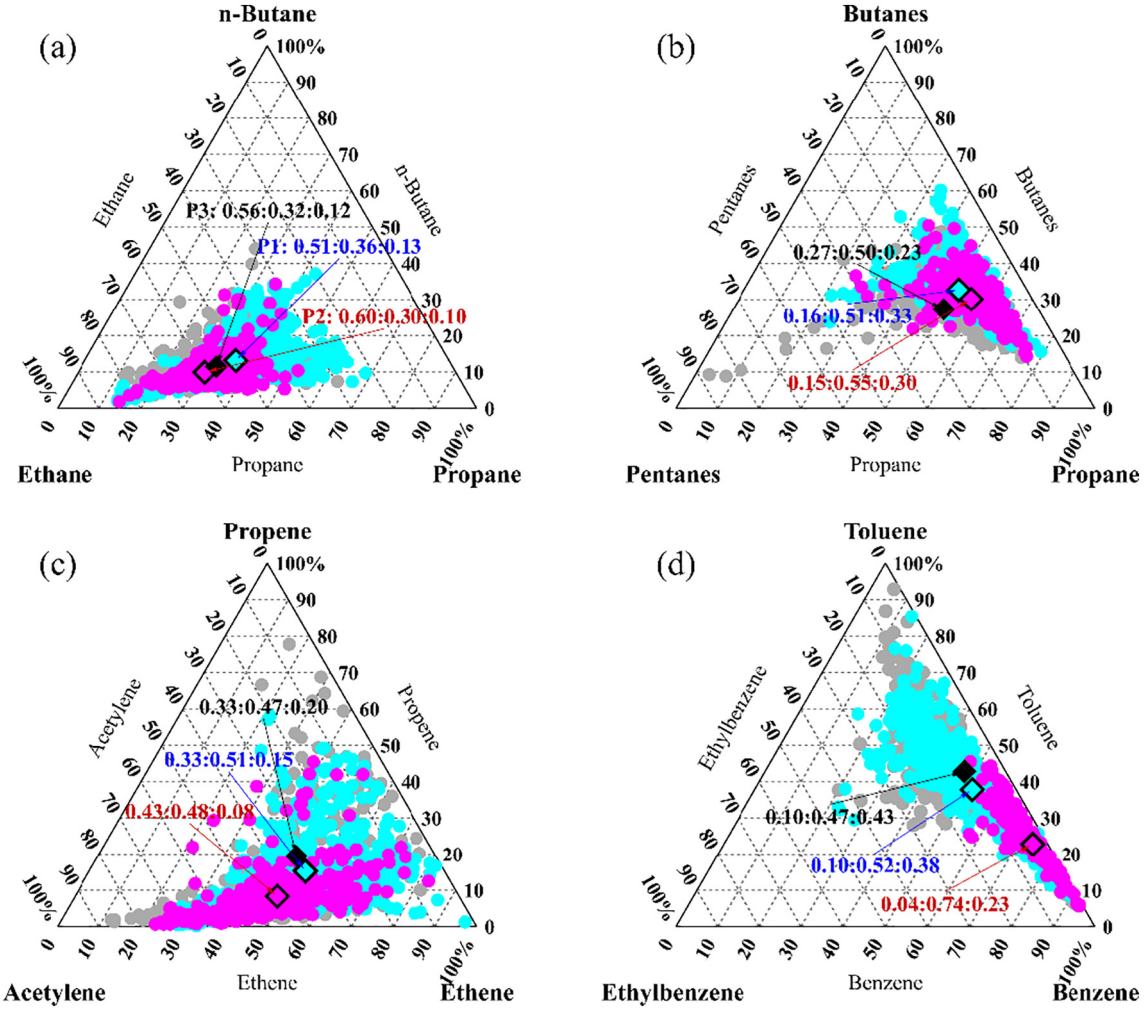

Fig. 4. Ternary plots and average ratios of (a) ethane/*n*-butane/propane, (b) pentanes/propane/butanes, (c) acetylene/ethene/propene, (d) ethylbenzene/benzene/toluene during P1, P2, and P3. The ratios mean relative fractions of average mixing ratios for NMHC species on left, right, and top vertexes of ternary plots.

P1 and P2 to 27% during P3 (Fig. 4b). This is possibly due to the relatively high temperature during P3 which is in favor of gasoline evaporation (Song et al., 2019). Average fraction of propene in the sum of acetylene, ethene, and propene during P2 was 8%, lower than values for P1 and P3 by factors of 2–2.5 (Fig. 4c). Petrochemical industry is an important source of ambient propene in Nanjing (Wang et al., 2020a), and therefore the lowest propene fraction during P2 indicates the possible decline of petrochemical industrial emissions due to COVID-19 lockdown. Average fraction of benzene in the sum of benzene, ethylbenzene, and toluene increased from 38% for P1 to 74% for P2 (Fig. 4d). Ratio of toluene/benzene (T/B) is often used to preliminary analyze relative importance of vehicular exhaust, industrial emission, and combustion sources (Zhang et al., 2016; Song et al., 2020). The average value of T/B during P2 was 0.32 ppb/ppb, significantly lower than values for P1 and P2 (0.73 ppb/ppb for P1 and 0.91 ppb/ppb for P2). One possible explanation for this finding is that relative decrease of average mixing ratio for toluene during P2 *versus* P1 (70%) was larger than that for benzene (30%). This indicates that sources of ambient toluene and benzene during P2 possibly changed due to COVID-19 lockdown, *i.e.* reduction of VOCs emissions from once source rich in toluene was larger than another source rich in benzene. Furthermore, it was found that T/B values for these three periods were all lower than emission ratio of T/B from vehicular emission (1.0–2.5 ppb/ppb) (Song et al., 2020) and paints use (>3 ppb/ppb) (Mo et al., 2016), but fell in the range of emission ratios for coal combustion and biomass burning (Zhang et al., 2016). Actually, residential coal/biomass combustion has been forbidden in Nanjing, and therefore the lower T/B values during P1-P3 may not be related to these combustion sources. Further analysis is needed to identify another VOCs sources which are rich in benzene.

3.2.2. NMHCs source apportionment using PMF

In this study, we focused on investigating changes in NMHCs sources caused by COVID-19 lockdown. The positive matrix factorization (PMF, version 5.0) model developed by the U.S. Environmental Protection Agency (EPA) was used to identify NMHC sources and calculate relative contributions for each individual source. Detailed introductions on principles and operations of PMF5.0 has been described in the user guide written by Norris et al. (2014). Briefly, PMF is a multi-factor analysis tool which can decompose the speciated NMHCs observation data matrix (X) into two matrices, including a matrix of factor contributions (G) and a matrix of factor profiles (F) (Eq. (1)):

$$x_{ij} = \sum_{k=1}^{p} g_{ik} f_{kj} + e_{ij} \quad (1)$$

where x_{ij} is the mixing ratio for j^{th} NMHC species in i^{th} sample; g_{ik} is the contribution of k^{th} factor to total mixing ratio of NMHCs in i^{th} sample; f_{kj} means the chemical profile of NMHCs (*i.e.* percentages of j^{th} NMHC species in total mixing ratios of NMHCs) for k^{th} factor; e_{ij} represents the residual for j^{th} NMHC species in i^{th} sample.

3.2.2.1. Settings of PMF. In this study, NMHC species with high mixing ratios, low measurement uncertainty, and strong indications on emission sources were given priority in selecting inputs for PMF. Finally, mixing ratios for total NMHCs and 35 individual species, including 18 alkanes, 10 aromatics, 6 alkenes, and acetylene, were inputted in PMF for source apportionment. The list of these species was shown in *x*-axis of Fig. 5. In base model runs of PMF, factors number was set as 3–8. Chemical profiles of resolved factors and Q_{true}/Q_{robust} values for each solution were compared with each other. Finally, the 5-factors solution was chosen to analyze ambient NMHCs sources, according to reasonability of physical explanations for individual factors. F_{peak} model runs were then conducted with F_{peak} values of ±1, ±0.5, and 0 to evaluate rotational ambiguity in PMF solutions. Results with F_{peak} of -1.0 were then selected based on *G-Space* plot. Additionally, bootstrap analysis with 100 runs were carried out to assess error and uncertainty of PMF solution. Average and median values for mixing ratios of individual NMHC species in each factor agreed well (Fig. S8 in Supplement), suggesting the stability of PMF solutions. Median result of 100 bootstrap runs was then used for identification of PMF-resolved factors and calculation of contributions from each source.

3.2.2.2. Identification of PMF-resolved factors. Fig. 5 shows chemical profiles of five PMF-resolved factors. Ethane, propane, and acetylene were the most abundant three species in factor 1 (F1), with percentages in total mixing ratios of 35 species of 40.0%, 22.6%, and 14.0%, respectively (Fig. 5a). F1 contributed 77.9%, 62.9%, and 85.6% of measured mixing ratios of ethane, propane, acetylene. Atmospheric lifetimes for these three species were estimated as 5–24 days with average OH concentration of 2×10^6 molecule/cm^3 according to their reaction rate constants with OH radical (k_{OH}) in the Master Chemical Mechanism (MCM) v3.3.1 (http://mcm.leeds.ac.uk/MCM/). Due to their long lifetimes in the atmosphere, these species could be influenced by long-distance transport of air masses and background air. Additionally, NMHCs levels contributed by F1 showed a significant correlation with $PM_{2.5}$ concentrations, with r of 0.61 (Fig. S9 of Supplement). Potential source region analysis by Li et al. (2020) suggested that $PM_{2.5}$ concentrations in the YRD region during January–March 2020 were largely influenced by transport from North China. Therefore, F1 was identified as a source related to *transport and background air masses*.

As described in Section 2, the NUIST site is close to largest industrial zone in Nanjing (A in Fig. 1). Benzene, ethene, propene, xylenes, and toluene are important products of petrochemical enterprises in this zone. Meanwhile, benzene is also used as a raw material to produce chlorobenzene and cyclohexane in a chemical enterprise. Since these species belong to different production lines, temporal variability of their ambient mixing ratios showed significant discrepancies, and therefore they were attributed to three PMF-resolved factors. Factor 2 (F2) was characterized by high abundance of benzene, with percentages in total 35 species of 32.7% and relative contribution of 75.4% (Fig. 5b). It was found that mixing ratios of benzene showed good correlations with cyclohexane and chlorobenzene ($r = 0.77$) (Fig. S10 of Supplement), but showed poor correlations ($r < 0.25$) with other aromatics (*e.g.* toluene, *m,p*-xylene), and therefore F2 was identified as a source mainly related to *chemical industry-benzene*. C2-C3 alkenes and C7-C9 aromatics were the most abundant species in factor 3 (F3) and factor 4 (F4), respectively. F3 contributed 84.3% and 31.5% of propene and ethene mixing ratios (Fig. 5c), while F4 contributed 57%–83% of C7-C9 aromatics (Fig. 5d). Light alkenes are important constitutes of NMHCs from petrochemical industry (Ryerson et al., 2003; Mo et al., 2015), and therefore F3 was considered as *petrochemical industry#1-propene/ethene*. Some studies reported that C7-C9 aromatics were major constitutes of NMHCs from paints and solvent use (Yuan et al., 2010; Li et al., 2019). However, there are few factories using a lot of solvents and paints near the NUIST site, and therefore F4 was also considered mainly related to petrochemical industry (*petrochemical industry#2-C7-C9 aromatics*).

Butanes and pentanes in factor 5 (F5) showed the two largest percentages in the summed mixing ratios of total 35 species, with respective values of 26.9% and 29.0% (Fig. 5e). Relative contributions of F5 to measured mixing ratios of butanes and pentanes reached 35.3% and 67.1%, respectively. C4-C5 alkanes are major constitutes of NMHCs from gasoline vapor and vehicular exhaust (Song et al., 2019), and therefore this factor was named as *gasoline evaporation and vehicular emission*.

3.2.2.3. Changes of NMHCs sources among P1, P2, and P3. Fig. 6 shows temporal variation of NMHCs sources during the entire observation periods. There were significant differences of NMHCs sources among P1, P2, and P3. *Transport and background air masses* was the largest contributor to NMHCs mixing ratios during P1 and P2, with respective values of 46% and 57%, while its relative contribution decreased to 35% during P3. The relative contribution from *petrochemical industry#1-propene/ethene* during P3 was only 4%, significantly lower than values for P1 (16%) and

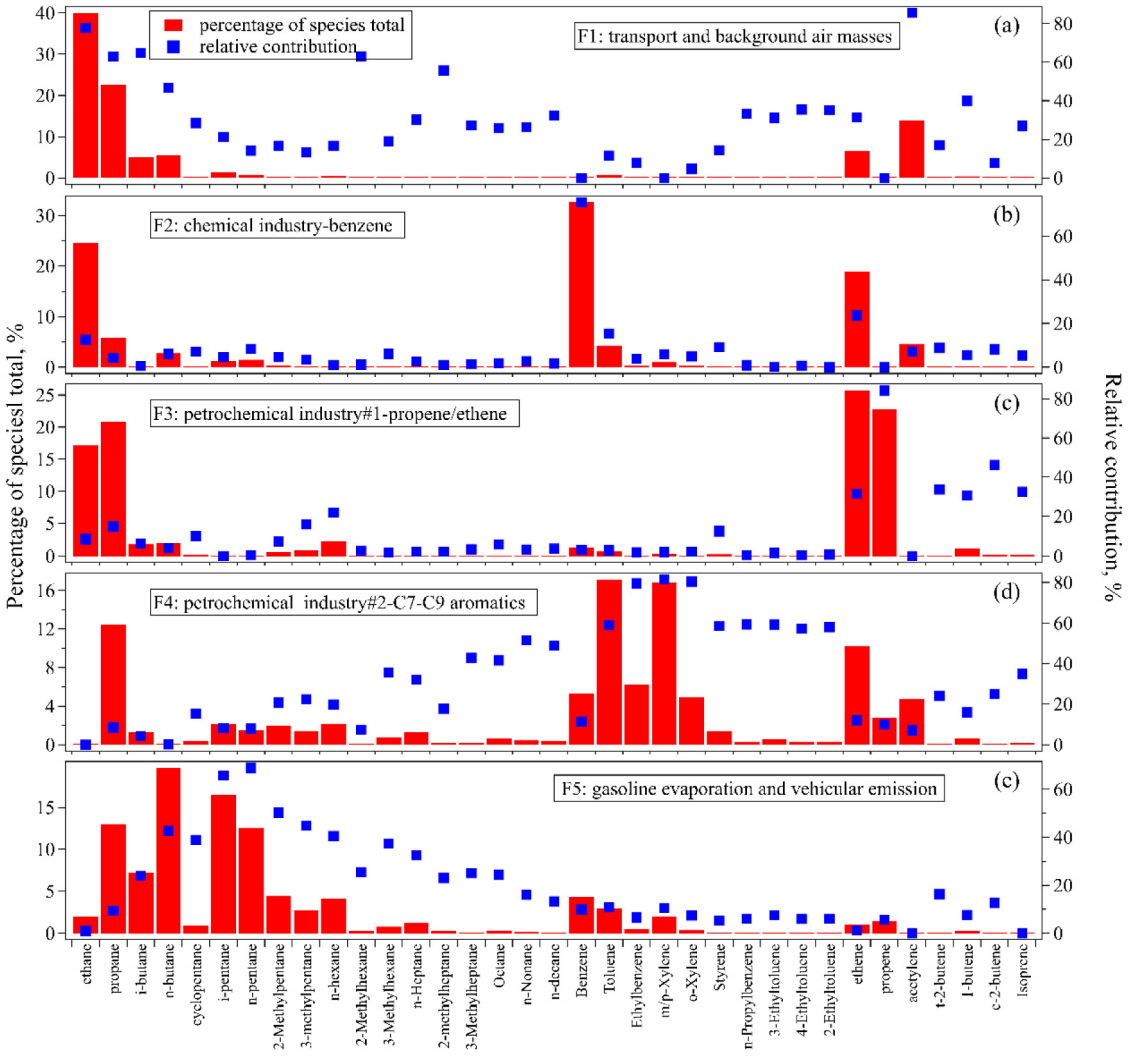

Fig. 5. Chemical profiles for five PMF-resolved factors. Blue filled squares mean percentages of individual species in total mixing ratios of 35 NMHCs species for each factor. Red bars mean relative contributions of each factor to measured mixing ratios for individual species.

P2 (10%). Instead, *petrochemical industry#2-C7-C9 aromatics* showed the highest relative contribution of 40% during P3, whereas its contributions during P1 and P2 were only 15% and 2%, respectively. For *chemical industry-benzene*, its relative contribution during P2 was 25%, higher than those for P1 (13%) and P3 (6%). The relative contribution from *gasoline evaporation and vehicular emission* during P2 was 7%, significantly lower than those for P1 (11%) and P3 (14%).

To further discuss possible causes for changes of NMHCs sources, average NMHCs levels contributed by each individual source during P1, P2, and P3 were compared in Fig. 6e. The average NMHCs mixing ratio from *transport and background air masses* during P1 was 17.5 ± 7.5 ppb, and decreased by 34% and 60% during P2 and P3, respectively. As shown in Table 1 and Fig. S4, meteorological conditions were similar between P1 and P2. Liu et al. (2020) quantitatively evaluated influences of meteorology and emission reduction on air quality changes in the YRD region during the COVID-19 lockdown period using Community Multiscale Air Quality (CMAQ) model. Results showed that emission reduction was the major driving force for the decrease of PM2.5 concentrations. NMHCs mixing ratios from F1 showed a significant correlation with PM2.5 concentrations ($r = 0.61$) at the level of 0.01 (Fig. S9 of Supplement). This indicated that the decrease of NMHCs mixing ratios from F1 during P2 *versus* P1 was also mainly caused by emission reduction during the COVID-19 lockdown period. The measurement study at the JEMC site in Nanjing during 2016 reported that ambient ethane and acetylene exhibited the highest levels in December and January, and decreased gradually to the lowest values in July–August (Wang et al., 2020a). Temporal changes of meteorological conditions are one possible explanation for the decrease of NMHCs levels from *transport and background air masses* during P3. Relatively higher boundary layer and wind speed during P3 would be in favor of dilution and diffusion of ambient NMHCs, meanwhile the high temperature and solar radiation could accelerate photochemical removal of NMHCs. Compared with reactive alkenes and aromatics, these long-lived species abundant in *transport and background air masses* were less affected by photochemical reactions. In addition, fuels (*e.g.* coal, natural gas, biomass) were consumed more for heating during winter. Although residential combustion of coal and biomass has been forbidden in Nanjing, these fuels were still heavily used for wintertime heating in rural areas of Jiangsu Province. Considering long-lived NMHC species could be transported a long distance (Fig. S5 of Supplement), the relatively high NMHCs levels during P1 and P2 were also possibly related to larger emissions from fuel combustion on a regional scale.

For the two sources related to petrochemical industry, their contributed NMHCs levels both showed the lowest values during P2. The relative declines of average NMHCs levels during P2 *versus* P1 for *petrochemical industry#2-C7-C9 aromatics* and *petrochemical industry#1-propene/ethene* reached 94% and 67%, respectively. NMHC levels from *gasoline evaporation and vehicular emission* also displayed the

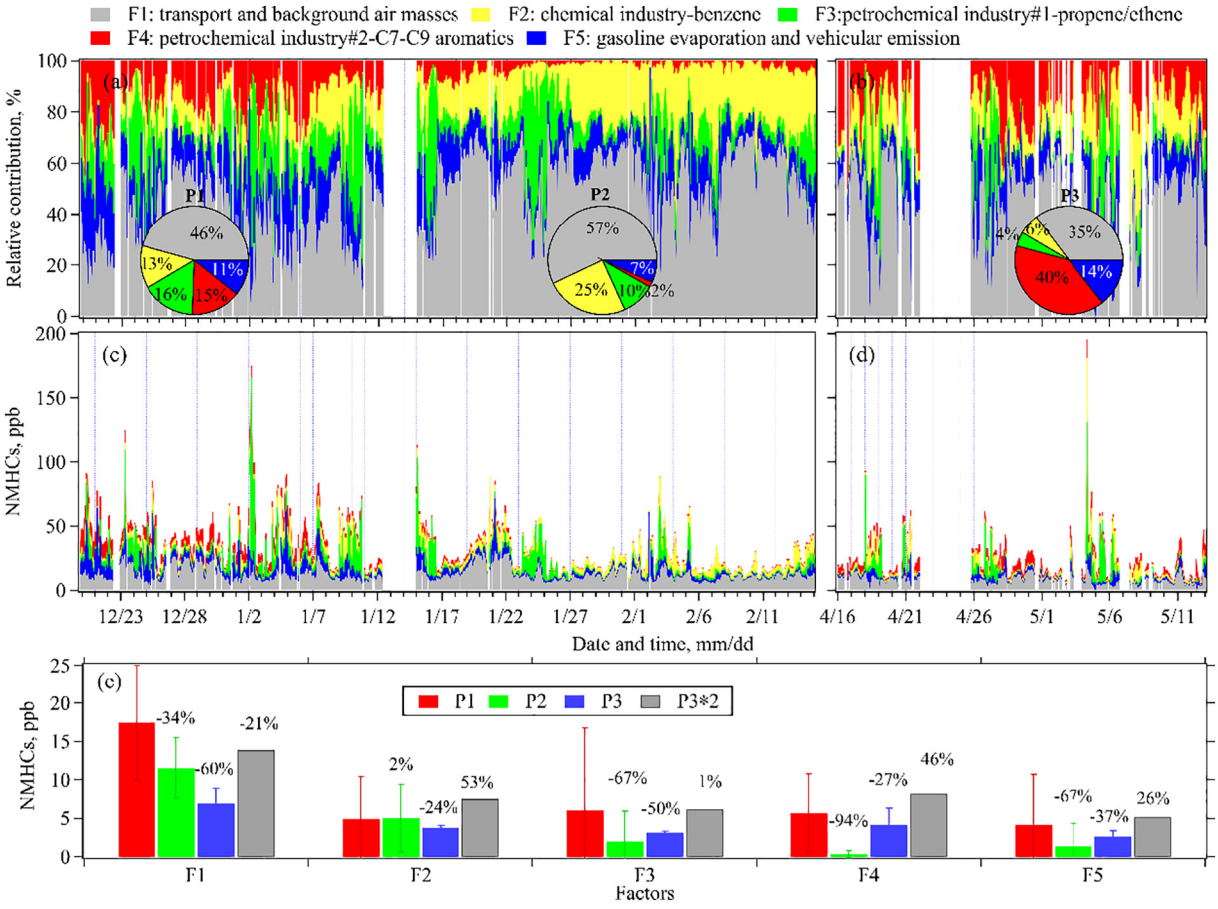

Fig. 6. Temporal changes in (a-b) relative contributions and (c-e) NMHCs mixing ratios from five PMF-resolved sources during P1-P3.

lowest average value during P2, with relative decline *versus* P1 of 67%. Considering changes of meteorological conditions and NMHCs background levels during P3, ambient mixing ratios of NMHCs during P3 were multiplied by 2, which was assumed according to the relative decline of NMHCs level from *transport and background air masses* during P3 *versus* P1 and the seasonal variability of long-lifetime NMHC species reported by Wang et al. (2020a). Average NMHCs levels from *petrochemical industry#2-C7-C9 aromatics*, *petrochemical industry#1-propene/ethene*, and *gasoline evaporation and vehicular emission* during P2 were lower than 2 times of values for P3 by factors of 4–42. The decreases of NMHCs mixing ratios from these three sources during P2 *versus* P1 and P3 were mainly related to the lockdown of industry and transportation caused by COVID-19. Different with the two sources related to petrochemical industry, average NMHCs levels from *chemical industry-benzene* did not show a significant decline during P2 *versus* P1. This might indicate that the chemical production line using benzene was little affected by COVID-19 lockdown.

To compare with reduction of VOCs emissions in the YRD region, changes in total NMHCs mixing ratios from three industrial sources (*i.e.* F2, F3, and F4) were calculated and compared with VOCs emissions from industrial processing reported by Li et al. (2020). Summed NMHCs levels from F2, F3, and F4 reduced by 56% during P2 *versus* P1, close to the relative reduction of VOCs emission from industrial processing (51%) during Level I response period *versus* pre-response period. VOCs emissions from vehicular exhaust and gasoline evaporation reduced by 75% and 50% during Level I and Level II response period, respectively (Li et al., 2020). In this study, NMHCs mixing ratios from *gasoline evaporation and vehicular emission* reduced by 67% during P2 *versus* P1, which agrees well with changes of transportation-related VOCs emissions reported by Li et al. (2020).

3.3. Ratios of NMHCs reactivity versus NO_2: implications for O_3 formation

Ambient NMHCs and NO_X are key precursors of ground-level O_3 formation, and ratios of NMHCs/NO_X will influence the sensitivity of O_3 formation, *i.e.* non-linear relationship of O_3 formation with NMHCs and NOx (Atkinson et al., 2006; Tan et al., 2019). Considering O_3 formation is not only related to NMHCs mixing ratios but also their reactivity, OH reactivity for total NMHCs species ($R_{OH,\ NMHCs}$) were calculated using the following equation:

$$R_{OH,NMHCs} = \sum [NMHC_i] \times k_{OH,NMHC_i} \quad (2)$$

where [$NMHC_i$] represents mixing ratio of the i^{th} NMHC species. $k_{OH,\ NMHC_i}$ means rate constant for the reaction of i^{th} NMHC species with OH radical. Values for $k_{OH,\ NMHC_i}$ are from MCM v3.3.1 (http://mcm.leeds.ac.uk/MCM/).

$R_{OH,NMHCs}$ exhibited a significant correlation with NO_2 levels during P2, with r of 0.31, but they had poor correlations during P1 and P3 ($r = 0.025$–0.058) (Fig. S11a of Supplement). This indicates that sources of ambient NMHCs and NO_2 were more similar during P2 than the other two periods. The relatively low standard deviation of $R_{OH,NMHCs}/NO_2$ also suggests the relatively stronger covariation of $R_{OH,NMHCs}$ with NO_2 during P2 (Fig. S11b of Supplement). One possible explanation for this result is that relative contributions of petrochemical industry to NMHCs decreased significantly during P2, and thus more NMHCs were from background or combustion sources. Average value of $R_{OH,\ NMHCs}$ during P2 was 1.94 s^{-1}, significantly lower than values for P1 (5.00 s^{-1}) and P3 (3.24 s^{-1}). Relative decrease of $R_{OH,\ NMHCs}$ during P2 *versus* P1 was 61%, higher than that for NMHCs mixing ratios (46%). This is because mixing ratios of reactive aromatics and alkenes showed

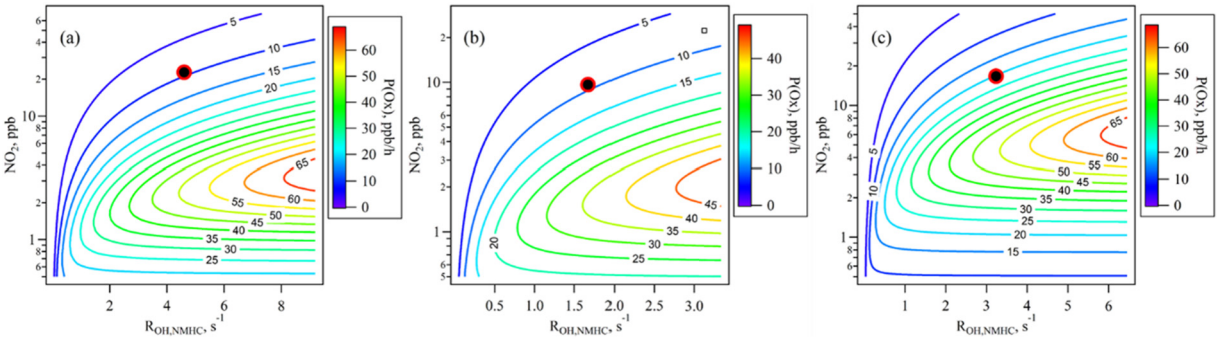

Fig. 7. Contour plots of total oxidant production rate ($P(O_X)$) as a function of NMHCs reactivity ($R_{OH,NMHCs}$) and NO_2 levels during (a) P1, (b) P2, and (c) P3.

higher declines than alkanes and alkynes (Fig. 3). As shown in Fig. S12 of Supplement, anthropogenic alkenes was the largest contributor to $R_{OH,NMHCs}$ during three periods, with fractions of 42.9%–52.6%, followed by alkanes (22.2%–27.6%), aromatics (15.6%–26.1%), isoprene (1.5%–9.0%), and acetylene (1.2%–2.7%).

Average ratios of $R_{OH,NMHCs}/NO_2$ during P1, P2, and P3 were 0.124 ± 0.175 s^{-1} ppb^{-1}, 0.087 ± 0.067 s^{-1} ppb^{-1}, and 0.093 ± 0.166 s^{-1} ppb^{-1}, respectively (Fig. S11b of Supplement). These values were then compared with monthly-averaged $R_{OH,NMHCs}/NO_2$ at the JEMC site which were calculated based on online measurements of NMHCs and NO_2 during 2016 (Wang et al., 2020a) (Fig. S13 of Supplement). Average values of $R_{OH,NMHCs}/NO_2$ during P1 and P2 were lower than those for January and February in 2016, respectively. One possible explanation for this phenomenon is that relative decline of VOCs emissions from industrial processing and solvent use (51%–100%) were larger than that for NOx (20%–29%) during COVID-19 lockdown period (Li et al., 2020).

Monthly-averaged $R_{OH,NMHCs}/NO_2$ at the JEMC site during 2016 showed a seasonal variation pattern with higher values during summer possibly due to the high temperature and solar radiation are favorable to VOCs emissions from vaporization and biogenic sources. According to O_3 sensitivity analysis results at the JEMC site during August 2016 using observation-based box model, O_3 formation was controlled by both NMHCs and NOx (Wang et al., 2020b). Average $R_{OH,NMHCs}/NO_2$ during August 2016 was 0.35 ± 0.29 s^{-1} ppb^{-1}, higher than values during P1-P3 by a factor of 3–4. This suggests that O_3 formation at the NUIST site during P1-P3 tend to be more sensitive to NMHCs.

Furthermore, O_X production rates ($P(O_X)$) at noon (10:00–14:00 LT) during P1, P2, and P3 were estimated based on $R_{OH,NMHCs}$ and NO_2 levels using a simplified model that calculated $P(O_X)$ by solving steady-state equations for OH, HO_2, and RO_2 radicals. More detailed descriptions on principles and assumptions of this model can be found in the paper by Zhang et al. (2014). In this method, concentrations of HO_2 and RO_2 were assumed to be equal. Although this assumption can be acceptable in Beijing (Liu et al., 2012), it maybe not true in Nanjing during December 2019-May 2020. Another uncertainty comes from influences of transport on O_3, NMHCs, and NO_X which were not considered in this model. The production rates of OH and HO_2 radicals ($P(HO_X)$) is an important parameter to calculate $P(O_X)$. In this study, its value during P3 was assumed to be 14 ppb h^{-1} according to the result of radical budget modelling in Beijing during summer of 2007 (Liu et al., 2012). The $P(HO_X)$ during P1 and P2 were assumed to be 7 ppb h^{-1} considering seasonality of HO_X abundance (Kanaya et al., 2007). It should be point out that there is large uncertainty in assuming $P(HO_X)$ values due to the lack of measurement and model results on HO_X radicals in Nanjing.

Contour plots of $P(O_X)$ with $R_{OH,NMHCs}$ and NO_2 during these three periods were compared in Fig. 7. Similar with preliminary results from $R_{OH,NMHCs}/NO_2$, O_3 formation at noon during P1-P3 were more sensitive to NMHCs and fell within NMHCs-limited regime (*i.e.* area above the black ridge line). Due to the high solar radiation and temperature during April–May, $P(O_X)$ during P3 was about twice of values for P1-P2. Interestingly, we found that $P(O_X)$ during P2 (9.2 ppb h^{-1}) did not show a significant decrease *versus* P1 (9.3 ppb h^{-1}) despite average $R_{OH,NMHCs}$ and NO_2 at noon during P2 dropped by 64% and 58%, respectively. This finding implies that effect of NMHCs reduction on O_3 control could be offset by NO_X reduction when O_3 formation is mainly controlled by NMHCs. Therefore, it is important to determine a scientific ratio of $R_{OH,NMHCs}/NO_2$ in the development of O_3 control policies.

4. Conclusions

To assess impact of COVID-19 lockdown on ambient VOCs levels and sources, mixing ratios of speciated VOCs were online measured by a GC-MSD/FID system at the NUIST site in Nanjing during December 20, 2019-Feburary 15, 2020 and April 15–May 13, 2020. Average mixing ratio of total measured VOCs during COVID-19 lockdown period (P2) decreased by 47%. Average levels for those species with long lifetime (*e.g.* CFCs, ethane, acetylene, benzene) showed lower relative declines (4%–32%) during P2 *versus* P1, whereas reactive aromatics and alkenes exhibited higher declines (49%–92%). The differences of relative decreases for individual VOC species levels suggest possible changes of VOCs sources during P2.

The PMF model was then applied for NMHCs sources apportionment and five sources were identified, including *transport and background air masses*, *chemical industry-benzene*, *petrochemical industry#1-propene/ethene*, *petrochemical industry#2-C7-C9 aromatics*, and *gasoline evaporation and vehicular emission*. Average NMHCs mixing ratios from *petrochemical industry#2-C7-C9 aromatics*, *petrochemical industry#1-propene/ethene*, and *gasoline evaporation and vehicular emission* all showed the lowest values during P2, with relative decreases *versus* P1 of 94%, 67%, and 67%, respectively. However, average NMHCs level from *chemical industry-benzene* did not exhibit a significant decline during P2. The relative reduction of summed NMHCs levels from these three industrial sources was 56% during COVID-19 lockdown period, close to the result for VOCs emissions from industrial processing (51%).

Ratios of $R_{OH,NMHCs}$ *versus* NO_2 levels and $P(O_X)$ were calculated to investigate O_3 formation regime. Average values of $R_{OH,NMHCs}/NO_2$ during P1, P2, and P3 were 0.124 ± 0.175 s^{-1} ppb^{-1}, 0.087 ± 0.067 s^{-1} ppb^{-1}, and 0.093 ± 0.166 s^{-1} ppb^{-1}, respectively. These values were lower than $R_{OH,NMHCs}/NO_2$ during August 2016 by 65%–75%, suggesting that O_3 formation tend to be more sensitive to NMHCs during P1-P3. Contour plots of $P(O_X)$ at noon with $R_{OH,NMHCs}$ and NO_2 also suggest that O_3 formation during P1-P3 fell in NMHCs-limited regime. Despite average $R_{OH,NMHCs}$ and NO_2 at noon during P2 dropped by 64% and 58% *versus* P1, $P(O_X)$ during P2 (9.2 ppb h^{-1}) was close to the value for P1 (9.3 ppb h^{-1}). This suggests it is important to design a scientific reduction scheme for NMHCs and NO_X in the development of O_3 control policies.

CRediT authorship contribution statement

Ming Wang: Methodology, Investigation, Data curation, Visualization, Writing – original draft. **Sihua Lu:** Validation, Investigation, Data

curation, Writing – review & editing. **Min Shao:** Conceptualization, Supervision, Project administration, Funding acquisition, Writing – review & editing. **Limin Zeng:** Investigation, Writing – review & editing. **Jun Zheng:** Investigation, Resources, Writing – review & editing. **Fangjian Xie:** Investigation, Writing – review & editing. **Haotian Lin:** Data curation, Formal analysis. **Kun Hu:** Data curation, Formal analysis. **Xingdong Lu:** Data curation.

Declaration of competing interest

The authors declare that they have no known competing financial interests or personal relationships that could have appeared to influence the work reported in this paper.

Acknowledgement

This work was supported by the National Key Research and Development Program of China (No. 2016YFC0202200) and the National Natural Science Foundation of China (No. 41505113).

Appendix A. Supplementary data

Supplementary data to this article can be found online at https://doi.org/10.1016/j.scitotenv.2020.143823.

References

An, J.L., Wang, J.X., Zhang, Y.X., Zhu, B., 2017. Source apportionment of volatile organic compounds in an urban environment at the Yangtze River Delta, China. Arch. Environ. Contam. Toxicol. 72, 335–348. https://doi.org/10.1007/s00244-017-0371-3.

Atkinson, R., Baulch, D.L., Cox, R.A., Crowley, J.N., Hampson, R.F., Hynes, R.G., Jenkin, M.E., Rossi, M.J., Troe, J., Subcommittee, I, 2006. Evaluated kinetic and photochemical data for atmospheric chemistry: volume II-gas phase reactions of organic species. Atmos. Chem. Phys. 6, 3625–4055. https://doi.org/10.5194/acp-6-3625-2006.

Baker, A.K., Beyersdorf, A.J., Doezema, L.A., Katzenstein, A., Meinardi, S., Simpson, I.J., Blake, D.R., Rowland, F.S., 2008. Measurements of nonmethane hydrocarbons in 28 United States cities. Atmos. Environ. 42 (1), 170–182. https://doi.org/10.1016/j.atmosenv.2007.09.007.

Bauwens, M., Compernolle, S., Stavrakou, T., Müller, J.-F., van Gent, J., Eskes, H., Levelt, P.F., van der .R., A, Veefkind, J.P., Vlietinck, J., Yu, H., Zehner, C., 2020. Impact of coronavirus outbreak on NO_2 pollution assessed using TROPOMI and OMI observations. Geophys. Res. Lett. 47, e2020GL087978. https://doi.org/10.1029/2020gl087978.

Chauhan, A., Singh, R.P., 2020. Decline in $PM_{2.5}$ concentrations over major cities around the world associated with COVID-19. Environ. Res. 187, 109634. https://doi.org/10.1016/j.envres.2020.109634.

Chen, Q.X., Huang, C.L., Yuan, Y., Tan, H.P., 2020. Influence of COVID-19 event on air quality and their association in Mainland China. Aerosol Air Qual. Res. 20, 1541–1551. https://doi.org/10.4209/aaqr.2020.05.0224.

Gentner, D.R., Worton, D.R., Isaacman, G., Davis, L.C., Dallmann, T.R., Wood, E.C., Herndon, S.C., Goldstein, A.H., Harley, R.A., 2013. Chemical composition of gas-phase organic carbon emissions from motor vehicles and implications for ozone production. Environ. Sci. Technol. 47, 11837–11848. https://doi.org/10.1021/es401470e.

Huang, X., Ding, A., Gao, J., Zheng, B., Zhou, D., Qi, X., Tang, R., Wang, J., Ren, C., Nie, W., Chi, X., Xu, Z., Chen, L., Li, Y., Che, F., Pang, N., Wang, H., Tong, D., Qin, W., Cheng, W., Liu, W., Fu, Q., Liu, B., Chai, F., Davis, S.J., Zhang, Q., He, K., 2020. Enhanced secondary pollution offset reduction of primary emissions during COVID-19 lockdown in China. Natl. Sci. Rev. https://doi.org/10.1093/nsr/nwaa137.

Kanaya, Y., Cao, R.Q., Akimoto, H., Fukuda, M., Komazaki, Y., Yokouchi, Y., Koike, M., Tanimoto, H., Takegawa, N., Kondo, Y., 2007. Urban photochemistry in central Tokyo: 1. Observed and modeled OH and HO_2 radical concentrations during the winter and summer of 2004. J. Geophys. Res.-Atmos. 112, D21312. https://doi.org/10.1029/2007jd008670.

Kondo Nakada, L.Y., Urban, R.C., 2020. COVID-19 pandemic: impacts on the air quality during the partial lockdown in Sao Paulo state, Brazil. Sci. Total Environ. 730, 139087. https://doi.org/10.1016/j.scitotenv.2020.139087.

Kumari, P., Toshniwal, D., 2020. Impact of lockdown measures during COVID-19 on air quality- a case study of India. Int. J. Environ. Health Res. 745, 141021. https://doi.org/10.1016/j.scitotenv.2020.141021.

Lelieveld, J., Evans, J.S., Fnais, M., Giannadaki, D., Pozzer, A., 2015. The contribution of outdoor air pollution sources to premature mortality on a global scale. Nature 525, 367–371. https://doi.org/10.1038/nature15371.

Li, M., Zhang, Q., Zheng, B., Tong, D., Lei, Y., Liu, F., Hong, C.P., Kang, S.C., Yan, L., Zhang, Y.X., Bo, Y., Su, H., Cheng, Y.F., He, K.B., 2019. Persistent growth of anthropogenic non-methane volatile organic compound (NMVOC) emissions in China during 1990-2017: drivers, speciation and ozone formation potential. Atmos. Chem. Phys. 19, 8897–8913. https://doi.org/10.5194/acp-19-8897-2019.

Li, L., Li, Q., Huang, L., Wang, Q., Zhu, A.S., Xu, J., Liu, Z.Y., Li, H.L., Shi, L.S., Li, R., Azari, M., Wang, Y.J., Zhang, X.J., Liu, Z.Q., Zhu, Y.H., Zhang, K., Xue, S.H., Ooi, M.C.G., Zhang, D.P., Chan, A., 2020. Air quality changes during the COVID-19 lockdown over the Yangtze River Delta region: an insight into the impact of human activity pattern changes on air pollution variation. Sci. Total Environ. 732, 139282. https://doi.org/10.1016/j.scitotenv.2020.139282.

Liu, Z., Wang, Y., Gu, D., Zhao, C., Huey, L.G., Stickel, R., Liao, J., Shao, M., Zhu, T., Zeng, L., Amoroso, A., Costabile, F., Chang, C.-C., Liu, S.-C., 2012. Summertime photochemistry during CAREBeijing-2007: ROx budgets and O_3 formation. Atmos. Chem. Phys. 12, 7737–7752. https://doi.org/10.5194/acp-12-7737-2012.

Liu, T., Wang, X., Hu, J., Wang, Q., An, J., Gong, K., Sun, J., Li, L., Qin, M., Li, J., Tian, J., Huang, Y., Liao, H., Zhou, M., Hu, Q., Yan, R., Wang, H., Huang, C., 2020. Driving forces of changes in air quality during the COVID-19 lockdown period in the Yangtze River Delta region, China. Environ. Sci. Technol. Lett. https://doi.org/10.1021/acs.estlett.0c00511.

Menut, L., Bessagnet, B., Siour, G., Mailler, S., Pennel, R., Cholakian, A., 2020. Impact of lockdown measures to combat Covid-19 on air quality over western Europe. Sci. Total Environ. 741, 140426. https://doi.org/10.1016/j.scitotenv.2020.140426.

Mo, Z., Shao, M., Lu, S., Qu, H., Zhou, M., Sun, J., Gou, B., 2015. Process-specific emission characteristics of volatile organic compounds (VOCs) from petrochemical facilities in the Yangtze River Delta, China. Sci. Total Environ. 533, 422–431. https://doi.org/10.1016/j.scitotenv.2015.06.089.

Mo, Z., Shao, M., Lu, S., 2016. Compilation of a source profile database for hydrocarbon and OVOC emissions in China. Atmos. Environ. 143, 209–217. https://doi.org/10.1016/j.atmosenv.2016.08.025.

Norris, G., Duvall, R., Brown, S., Song, B., 2014. EPA Positive Matrix Factorization (PMF) 5.0 Fundamentals and User Guide. U.S. Environmental Protection Agency.

Rodriguez-Urrego, D., Rodriguez-Urrego, L., 2020. Air quality during the COVID-19: PM2.5 analysis in the 50 most polluted capital cities in the world. Environ. Pollut. 266, 115042. https://doi.org/10.1016/j.envpol.2020.115042.

Ryerson, T.B., Trainer, M., Angevine, W.M., Brock, C.A., Dissly, R.W., Fehsenfeld, F.C., Frost, G.J., Goldan, P.D., Holloway, J.S., Hubler, G., Jakoubek, R.O., Kuster, W.C., Neuman, J.A., Nicks, D.K., Parrish, D.D., Roberts, J.M., Sueper, D.T., 2003. Effect of petrochemical industrial emissions of reactive alkenes and NOx on tropospheric ozone formation in Houston, Texas. J. Geophys. Res.-Atmos. 108, 4294. https://doi.org/10.1029/2002jd003070.

Sicard, P., De Marco, A., Agathokleous, E., Feng, Z., Xu, X., Paoletti, E., Rodriguez, J.J.D., Calatayud, V., 2020. Amplified ozone pollution in cities during the COVID-19 lockdown. Sci. Total Environ. 735, 139542. https://doi.org/10.1016/j.scitotenv.2020.139542.

Song, C., Liu, B., Dai, Q., Li, H., Mao, H., 2019. Temperature dependence and source apportionment of volatile organic compounds (VOCs) at an urban site on the north China plain. Atmos. Environ. 207, 167–181. https://doi.org/10.1016/j.atmosenv.2019.03.030.

Song, C., Liu, Y., Sun, L., Zhang, Q., Mao, H., 2020. Emissions of volatile organic compounds (VOCs) from gasoline- and liquified natural gas (LNG)-fueled vehicles in tunnel studies. Atmos. Environ. 234, 117626. https://doi.org/10.1016/j.atmosenv.2020.117626.

Tan, Z., Lu, K., Jiang, M., Su, R., Wang, H., Lou, S., Fu, Q., Zhai, C., Tan, Q., Yue, D., Chen, D., Wang, Z., Xie, S., Zeng, L., Zhang, Y., 2019. Daytime atmospheric oxidation capacity in four Chinese megacities during the photochemically polluted season: a case study based on box model simulation. Atmos. Chem. Phys. 19, 3493–3513. https://doi.org/10.5194/acp-19-3493-2019.

Wang, M., Zeng, L., Lu, S., Shao, M., Liu, X., Yu, X., Chen, W., Yuan, B., Zhang, Q., Hu, M., Zhang, Z., 2014. Development and validation of a cryogen-free automatic gas chromatograph system (GC-MS/FID) for online measurements of volatile organic compounds. Anal. Methods 6, 9424–9434. https://doi.org/10.1039/C4AY01855A.

Wang, M., Qin, W., Chen, W., Zhang, L., Zhang, Y., Zhang, X., Xie, X., 2020a. Seasonal variability of VOCs in Nanjing, Yangtze River delta: implications for emission sources and photochemistry. Atmos. Environ. 223, 117254. https://doi.org/10.1016/j.atmosenv.2019.117254.

Wang, M., Chen, W., Zhang, L., Qin, W., Zhang, Y., Zhang, X., Xie, X., 2020b. Ozone pollution characteristics and sensitivity analysis using an observation-based model in Nanjing, Yangtze River Delta region of China. J. Environ. Sci. 93, 13–22. https://doi.org/10.1016/j.jes.2020.02.027.

Yuan, B., Shao, M., Lu, S.H., Wang, B., 2010. Source profiles of volatile organic compounds associated with solvent use in Beijing, China. Atmos. Environ. 44, 1919–1926. https://doi.org/10.1016/j.atmosenv.2010.02.014.

Zangari, S., Hill, D.T., Charette, A.T., Mirowsky, J.E., 2020. Air quality changes in New York City during the COVID-19 pandemic. Sci. Total Environ. 742, 140496. https://doi.org/10.1016/j.scitotenv.2020.140496.

Zhang, Q., Yuan, B., Shao, M., Wang, X., Lu, S., Lu, K., Wang, M., Chen, L., Chang, C., Liu, S., 2014. Variations of ground-level O_3 and its precursors in Beijing in summertime between 2005 and 2011. Atmos. Chem. Phys. 14, 6089–6101. https://doi.org/10.5194/acp-14-6089-2014.

Zhang, Z., Zhang, Y., Wang, X., Lü, S., Huang, Z., Huang, X., Yang, W., Wang, Y., Zhang, Q., 2016. Spatiotemporal patterns and source implications of aromatic hydrocarbons at six rural sites across China's developed coastal regions. J. Geophys. Res.-Atmos. 121. https://doi.org/10.1002/2016JD025115.

Zhao, Y., Mao, P., Zhou, Y., Yang, Y., Zhang, J., Wang, S., Dong, Y., Xie, F., Yu, Y., Li, W., 2017. Improved provincial emission inventory and speciation profiles of anthropogenic non-methane volatile organic compounds: a case study for Jiangsu, China. Atmos. Chem. Phys. 17, 7733–7756. https://doi.org/10.5194/acp-17-7733-2017.

Zhao, Y., Zhang, K., Xu, X., Shen, H., Zhu, X., Zhang, Y., Hu, Y., Shen, G., 2020. Substantial changes in nitrogen dioxide and ozone after excluding meteorological impacts during the COVID-19 outbreak in Mainland China. Environ. Sci. Technol. Lett. 7, 402–408. https://doi.org/10.1021/acs.estlett.0c00304.